The Construction and Use of Toughness Maps in a
Fracture Analysis of the Micromechanics of a
Composite Failure

Cambridge Univ. (England)

Feb 81

19960223 114

DEPARTMENT OF DEFENSE
PLASTICS TECHNICAL EVALUATION CENTER
ARRADCOM, DOVER, N. J.

PLASTEC

CAMBRIDGE UNIVERSITY

Engineering Department

BIBLIOGRAPHIC INFORMATION

Analytical expressions are presented which predict the
debonding and pull-out lengths observed in brittle fibre
composites. These characteristic lengths are combined with
models of four toughening mechanisms to calculate the work
of fracture of a composite.

i

THE CONSTRUCTION AND USE OF
TOUGHNESS MAPS IN A
FRACTURE ANALYSIS OF THE MICRO-
MECHANICS OF A COMPOSITE FAILURE

J.K. Wells
and
P.W.R. Beaumont

ABSTRACT

Analytical expressions are presented which predict the debonding
and pull-out lengths observed in brittle fibre composites. These charac-
teristic lengths are combined with models of four toughening mechanisms
to calculate the work of fracture of a composite. The results are pre-
sented as maps showing not only contours of toughness but also the domi-
nant toughening micromechanism. The toughness is largely determined by
six material parameters, each map demonstrating the combined effect of
changing two of these simultaneously.

Maps are presented for glass-fibres in epoxy and carbon-fibres in
epoxy. Their use is demonstrated by showing the effects of hygrothermal
aging on the toughness of the composites.

NOMENCLATURE

A	Value of P just less than one
B	Value of P just greater than zero
d	Fibre diameter
E_f	Tensile modulus of fibre
$g(\ell)$	General probability distribution of ℓ
G_{II}	Critical strain energy release rate for mode 2 fibre/matrix bond failure
G_2	G_{II} divided by geometry factor α
G_m	Shear modulus of matrix
ℓ_d	Total debonded length of fibre
ℓ_m	Maximum pull-out length
$\bar{\ell}_p$	Mean pull-out length
$\bar{\ell}$	Average value of a distributed length, ℓ
m	Weibull modulus
P	Cumulative probability of failure
S	Cumulative probability of survival
W_e	Elastic work (per fibre)
W_i	Surface energy of fibre/matrix interface (per fibre)
W_p	Pull-out work (per fibre)
W_{pdf}	Post debond friction work (per fibre)
x	General distance from debond crack
x_c	Value of x which only a fraction B of pull-out lengths can exceed
α	Geometry factor from integration of stress field around fibre
β	Constant, but exact value depends on author
γ	Surface energy of the composite
γ_m	Surface energy of the matrix

NOMENCLATURE (cont.)

ϵ_f Failure strain of fibre

ϵ_m Failure strain of matrix

η Parameter dependent only on the Weibull modulus

σ_1, σ_2 Stresses at which fractions A, B of fibres have broken

σ_d Debond stress

σ_f Average fibre strength

σ_o Characteristic strength of fibre

τ_o Shear strength of fibre/matrix adhesive bond

τ_f Frictional shear stress

1. INTRODUCTION

A number of theories have been proposed to account for the origins of toughness of fibrous composites. This paper describes four models based on the debonding, fracture and pulling-out of fibres. An equation is derived for each fracture process which includes terms for the properties of the fibre, matrix and interface, together with the fibre debond length and fibre pull-out length. The fibre debond length and pull-out length are in turn predicted, allowing for the statistical distribution of fibre strength. The paper attempts to couple our understanding of the micromechanisms of fracture with the models for each fracture process, and thereby predict the range of dominance of each mode of fracture, and the corresponding toughness. This is done by constructing toughness maps in which the axes are, for example, fibre strength and interfacial shear stress. By plotting contours of toughness predicted using the models for each micromechanism of fracture, the effect of changing the material parameters on composite toughness can be displayed using the diagrams. As an example, the effect of hostile environments on composite fracture behaviour are analysed using the maps.

2. THEORY OF FIBRE DEBONDING

2.1 Prediction of Fibre Debonding Stress

A number of workers have considered the debonding of fibres in composite materials [1,2,3,4,5]. One approach [1,2,3,4] is to consider the stress carried by the fibre for which the corresponding interfacial shear stress exceeds the shear strength of the fibre/matrix interface, τ_o. In this case the debonding stress, σ_d, is given by:

$$\sigma_d = \beta \ \tau_o \ (\frac{E_f}{G_m})^{\frac{1}{2}} \qquad\qquad (1)$$

The value of the dimensionless constant β varies according to the details of the analysis, but is independent of fibre radius, $\cdot$, in all cases. Alternatively, the debonding stress may be determined by considering the energetics of the debonding process. When the interfacial shear crack propagates an increment δx, the energy balance demands that the surface energy of the new interface equals the strain energy released from the relaxed matrix (Fig. 1):

$$2\pi r \ G_{II} \ \delta x = \frac{1}{2} \frac{\sigma_d}{E_m} \ \delta V_m$$

The term δV_m is the effective incremental volume of matrix which is relaxed. Whilst δV_m must be proportional to the fibre area and the increment δx, its exact value can only be calculated from a full stress analysis around the fibre. For the purposes of this work, a dimensionless constant α is introduced such that:

$$\delta V_m = \alpha \ \pi r^2 \ \delta x$$

The debonding stress is therefore given by:

$$\sigma_d = (\frac{4E_m \ G_{II}}{\alpha r})^{\frac{1}{2}} \qquad\qquad (2)$$

For convenience, let $G_{II}/\alpha = G_2$, where G_2 may be determined experimentally.

Equation (2) may be compared with the expression derived by Outwater and Murphy [5]:

$$\sigma_d = (\frac{4E_f \ G_{II}}{r})^{\frac{1}{2}}$$

The dependence on E_f arises because Outwater and Murphy considered the released strain energy to come from the fibre.

Note that the energy-based calculations predict a debond stress which is a function of fibre radius, while equation (1) suggests that r and σ_d are independent.

Several workers [1,3,6] have conducted model experiments to study the debonding of wires or fibres but have not studied the effect of fibre size. In order to investigate the validity of equations (1) and (2) cold-drawn steel wires of two different diameters, were embedded in a Ciba-Geigy epoxy system (LY567/HY567), and the load to debond the wire measured.

Preliminary results show the debond stress is dependent on fibre diameter, which equation (1) fails to predict (Table 1). Equation (2) predicts a debond stress ratio for small:large wires of about 1.9, whereas a ratio of 2.4 was observed in the experiments. The difference in the two values lies within the limits of experimental error for the small number of specimens tested. The energy-based calculation of debonding stress therefore appears the more accurate.

In similar experiments, using bundles of 1600 glass fibres of 14 μm diameter, the debonding stress was estimated to be 0.6 ($\pm$ 0.1) GPa. If the modulus of the matrix, E_m, is 3 GPa, then G_2 has a value of about 210 joules/metre^2.

2.2 Prediction of the Fibre Debond Length

When the fibre stress exceeds the debonding stress an interfacial shear, or debond, crack propagates along the fibre. After debonding, the stress transfer between fibre and matrix is no longer by the shear

deformation of the matrix, but is due to frictional shear stresses between matrix and fibre. This stress is assumed to have a constant value, τ_f; in reality it will vary due to the Poisson contraction of the fibre within the matrix. The stress build-up is therefore assumed to be linear with increasing distance away from the debond crack (Figure 1).

The stress in the fibre is:

$$\sigma = \sigma_d + \frac{4\,\tau_f\,x}{d} \qquad (3)$$

Debonding will proceed until σ reaches the tensile strength of the fibre σ_f, and the total debonded length is then given by:

$$\boxed{\ell_d = \frac{d}{2\tau_f}\,(\sigma_f - \sigma_d)} \qquad (4)$$

3. THEORY OF FIBRE PULL-OUT

In the above discussion, no allowance was made for the distribution of flaws in the fibre, and the corresponding variation in strength. The fibre would therefore be expected to break in the region of maximum stress; that is, where the fibre emerges from the matrix.

3.1 Existing Calculation of Fibre Pull-Out Length

Some workers [5,7,8] consider the maximum pull-out length to be equal to half the critical fibre length. Whilst this forms an approximate upper bound on ℓ_m, it is not able to predict the pull-out length from materials properties.

3.2 New Calculation of Fibre Pull-Out Length

The variation of fibre strength is known to be well described by the Weibull distribution [9]. The cumulative probability of a fibre surviving a stress σ is given by:

$$S = \exp\left(-\left(\frac{\sigma}{\sigma_o}\right)^m\right) \qquad (5)$$

and the cumulative probability of failure by:

$$P = 1 - S$$

A more refined calculation of the pull-out length is made as follows. Since the variation of the fibre axial stress, given by equation (3), is a linear function of x, the pull-out length must also be of a Weibull distribution. Long pull-out lengths occur because there is a small probability of finding a severe flaw away from − in preference to a minor flaw near − the region of maximum stress.

Figure 2 shows how the variability in fibre strength leads directly to the possibility of fibre pull-out. If σ_1 is the stress at which a fraction A $(\leqslant 1)$ of fibres have fractured, and σ_2 is such that a fraction B $(\gtrsim 0)$ have broken, then a good estimate of the maximum pull-out length possible, ℓ_m, is given by:

$$\ell_m = \frac{\ell_d}{2} - x_c$$

The fractions A and B may be regarded as a measure of the shortest and longest lengths of fibre which can be resolved in experiments. This treatment assumes that the whole spectrum of flaws are repeated in a length of fibre which is small by comparison with the pull-out length.

The difference in the stresses σ_1 and σ_2 may be calculated from equation (3) giving:

$$(\sigma_1 - \sigma_2) = \frac{4\tau_f \ell_m}{d} \qquad (6)$$

The difference $(\sigma_1 - \sigma_2)$ is a function of the variability in the strength of fibres. For a fibre of uniform strength $(\sigma_1 - \sigma_2)$ would reduce to zero; for a fibre of variable strength, it may be calculated from equation (5) since:

$$-\frac{1}{m} \ln S = \frac{\sigma}{\sigma_o}$$

hence:

$$(\sigma_1 - \sigma_2) = \frac{\sigma_o}{m} (\ln \frac{A}{B}) \qquad (7)$$

The stress σ_o is the characteristic strength of the fibres, and is related to the mean strength, σ_f, by:

$$\sigma_o = \frac{\sigma_f}{(\ln 2)^{1/m}} \qquad (8)$$

Equating (6) and (7) and substituting for σ_o from equation (8):

$$\frac{\sigma_f}{m (\ln 2)^{1/m}} \ln (\frac{A}{B}) = \frac{4\tau_f \ell_m}{d} \qquad (9)$$

Rearranging equation (9) to find the average pull-out length $\overline{\ell}_p$, which is one half of the maximum pull-out length, ℓ_m;

$$\overline{\ell}_p = \frac{\sigma_f d}{8\tau_f} \cdot \eta \qquad (10)$$

where
$$\eta = \frac{\ell n\ (A/B)}{m\ (\ell n\ 2)^{1/m}}$$

η may be found from experiment; although A and B might be estimated from the shortest and longest experimentally resolved pull-out lengths. The Weibull modulus, m, may be found from experiment. Figure 3 shows pull-out and debond length data collected from 90 experiments on the fracture of glass-fibres in epoxy, similar to those described by Kirk, Munro and Beaumont [10]. These experiments were initially conducted for other purposes, but the results may be used to give an estimate of η. From equations (4) and (10), the slope of the graph is given by:

$$\frac{\ell_d}{\overline{\ell}_d} = \frac{4\ (1 - \frac{\sigma_d}{\sigma_f})}{\eta}$$

If σ_f and σ_d are assumed constant, having values of 1.65 and 0.6 GPa respectively, then η has a value of about 0.13. The data-points lying above the line are generally from low temperature experiments where debonding was encouraged; those below are from specimens which had been exposed to moisture. The value of η is dependent only on the reciprocal of the Weibull modulus of the fibre.

4. WORK OF FRACTURE

The work of fracture of glass-fibres in epoxy is thought to originate from four micromechanisms of fracture [10,11].

4.1 Post Debond Friction Energy

The Post Debond Friction work [12] is due to the relative slip of
the broken matrix over the debonded length of fibre, prior to the
failure of the fibre. The work done per fibre is given by:

$$Wpdf = \frac{\pi d \; \tau_f \; \ell_d^2 \; (\epsilon_f - \epsilon_m)}{2} \qquad (11)$$

The difference in fibre and matrix failure strains, $(\epsilon_f - \epsilon_m)$, may
be estimated as the ratio of fibre strength to fibre modulus for a
brittle matrix composite.

4.2 Elastic Energy in the Fibre

The fibre stress within the debonded region is reduced after
fibre failure. There is a corresponding release of elastic strain
energy from the fibre, which cannot assist in crack propagation.
The strain energy, sometimes called Elastic or Debond energy, was
first considered by Outwater and Murphy [5], and is given by:

$$W_e = \frac{\pi r^2}{E_f} \int_0^{\frac{\ell_d}{2}} \left| \sigma_f - \frac{2\tau_f \; x}{r} \right|^2 dx$$

$$= \frac{\pi r^2}{E_f} \left| \frac{\sigma_f^2 \; \ell_d}{2} + \frac{\tau_f^2 \; \ell_d^3}{6r^2} - \frac{\tau_f \; \sigma_f \; \ell_d^2}{2r} \right| \text{ per fibre} \qquad (12)$$

In order to simplify the above expression, it is often assumed that
the debond length is equal to the critical length. Equation (11)
then reduces to:

$$W_e = \frac{\pi r^2 \; \sigma_f^2 \; \ell_d}{6E_f} \qquad (13)$$

Since the debond stress has been shown to be a significant proportion of the fibre strength, the simplification is invalid. The full version of equation (12) should therefore be used.

4.3 Interfacial Surface Energy

The newly created interface between fibre and resin has an associated surface energy. This may be estimated by the product of the area of interface and the surface energy of the matrix, γ_m.

$$W_i = \pi d \, \ell_d \, \gamma_m \qquad \text{per fibre} \tag{14}$$

Wagner et al. [13] report a value of 100 J m^{-2} for γ_m.

4.4 The Work of Fibre Pull-Out

The work to pull a broken fibre a distance ℓ out of its matrix socket is given by:

$$W_p(\ell) = \frac{\pi d \, \tau_f \, \ell^2}{2}$$

Kelly [12] considered the average work of pull-out for fibres of length between zero and ℓ_m to be:

$$\overline{W}_p = \frac{1}{\ell_m} \int_0^{\ell_m} W_p(\ell) \, d\ell$$

This assumes a uniform probability of observing pull-out lengths between the two limits. Work by Beaumont and Anstice [14] has shown that both pull-out and debond lengths are well described by a Weibull probability function.

The calculation of the average work of pull-out requires the calculation of the average value of the square of the pull-out length. Similarly, the average Elastic Energy is a function of $\overline{\ell_d}$, $\overline{\ell_d^2}$ and $\overline{\ell_d^3}$ (eqn. 12).

If the cumulative probability distribution of lengths is of the form:

$$S = \exp\left(-\left(\frac{\sigma}{\sigma_o}\right)^m\right)$$

then the probability of observing a length between ℓ and $(\ell + d\ell)$ is:

$$g(\ell)\ d\ell = \frac{dS}{d\ell}\ d\ell = \frac{m\ \ell^{(m-1)}}{\ell_o^m}\ \exp\left(-\left(\frac{\ell}{\ell_o}\right)^m\right)\ d\ell$$

The averages of the pull-out and debond lengths are given by the general relations:

$$\overline{\ell} = \int_0^\infty \ell\ g(\ell)\ d\ell \qquad \overline{\ell^2} = \int_0^\infty \ell^2\ g(\ell)\ d\ell \qquad \overline{\ell^3} = \int_0^\infty \ell^3\ g(\ell)\ d\ell$$

The required integrals have been evaluated numerically, and, for convenience, are expressed as a power relationship of the Weibull modulus. The expressions shown in Table 2 approximate to the behaviour of the average over the stated range of Weibull moduli.

The correction factor for the pull-out term is particularly important. From equation (10), the average length of pull-out is proportional to the reciprocal of m; the work of pull-out is proportional to the square of the pull-out length. The resulting dependence of W_p on m is therefore given by the approximation:

$$W_p \propto \frac{1}{m^{(2.64)}}$$

In the case of the debond length, the distinction between $\overline{\ell^2}$ and $(\overline{\ell})^2$ is small, and probably negligible when considering Post Debond Friction. However, it may be important in the calculation of the elastic work where the difference of two variables is involved.

4.5 Other Toughening Mechanisms

There are other mechanisms of toughening which may also operate in GFRP, including the creation of fibre and matrix fracture surface and their associated surface energies. These are small by comparison with the major toughening mechanisms.

5. THE CONSTRUCTION AND IMPLICATIONS OF TOUGHNESS MAPPING

The complex interactions of material parameters cannot easily be seen from a set of equations; a mapping technique is therefore used to present the results. A map shows the effect of changing two material parameters simultaneously, such as fibre strength and interfacial shear stress. In addition, the principal toughening mechanism may be found for any combination of material parameters.

The maps are constructed by calculating pull-out and debond lengths, from equations (4) and (10), for particular combinations of material properties. These results may then be used to calculate the expected toughness of the chosen composite, using equations (11), (12), (13) and (14), together with the results in Table 2.

By dividing the total work of fracture per fibre by twice the area of the fibre and multiplying by the fibre volume fraction, the energy per unit area of crack extension, γ, is found.

5.1 Exposure of Glass-Fibre Reinforced Epoxy to Moisture

Contours of γ are plotted for variation of fibre strength and interfacial shear stress (Fig. 4), all other material parameters are held at the values listed in Table 3. In addition, to facilitate comparison with experimental data, contours of predicted debond lengths are plotted for the same variables (Fig. 5).

These maps apply to unidirectional glass-fibre reinforced epoxy such as have been tested by Anstice and Beaumont [15]. As an example, they are used in this work to account for the fracture behaviour of the specimens when exposed to a 100 °C/95 % RH environment.

Let us assume that the initial changes in debond length are caused by resin volume changes due to moisture uptake, and further, that the fibre strength is unaffected until cessation of resin swelling occurs after 3 days exposure.

The trajectory of the sample on the σ_f, τ_f plane is shown in Figures 4 and 5. Figure 6 shows the predicted and observed changes in γ. The prediction follows the trend well, despite the crude assumptions made. The absolute value of γ is lower than the experimental value because a small error in σ_f would cause a large error in γ, since γ is very sensitive to changes in σ_f. The interfacial properties may also be affected, but there is ambiguity in the interpretation of changing debond lengths; these may be caused by changes in both debonding stress (hence G_2) and τ_f. All reasonable combinations of G_2 and τ_f give approximately equal predicted toughness.

Figure (7) shows four toughness maps for glass-fibre in epoxy. They show, quantitatively, how all the complex interdependencies of material parameters combine to affect toughness. They may be summarised as follows:

i) toughness increases rapidly with increasing fibre strength;

ii) toughness decreases rapidly with increasing frictional shear stress;

iii) toughness decreases slowly with increasing fibre modulus and G_{II}.

In addition, the toughness is approximately proportional to the square of the fibre diameter, assuming that fibre-strength is independent of diameter.

5.2 Exposure of Carbon-Fibre Reinforced Epoxy to Moisture

Similar maps have been produced for carbon-fibre composites, Figures (8,9). These contour maps are again compared with results from (14). In the absence of data on the debonding stress of carbon fibres, a value of G_2 was chosen which gave good agreement with the observed toughness and pull-out length for the first data point. A value of $1950 \ Jm^{-2}$ was used for G_2. This corresponds to a debond stress of 2.4 GPa, and a typical debond length of less than one milli-metre. Debonding is not as easily observed in carbon-fibre composites as in glass-fibre. This is partly due to the short debond lengths in-volved, and the different optical properties of the fibre.

The changes in pull-out length and toughness which were observed by Anstice and Beaumont cannot be due to the same mechanism as proposed for the case of glass-fibre. The decreasing pull-out length observed for CFRP exposed to 100 °C/95° RH is due to an increase in τ_c. This

combined with a fall in G_2 from 1950 to ~ 1250 Jm^{-2} during the 28 days of the experiment, accounts for the observed change in toughness (Figs. 6 and 8).

6. CONCLUSIONS

i) The energy debonding stress of a fibre appears to be more accurately described by an energy-based calculation.

ii) The pull-out lengths of a brittle-fibre composite are directly related to the flaw distribution in the material.

iii) The toughness of GFRP and CFRP is due to four major sources which depend on six material constants $(\sigma_f, E_f, d, G_2, V_f, \tau_f)$. The debond stress is also a slow function of matrix modulus.

iv) The changes in the toughness of composites exposed to humid environments has been accounted for using plausible changes in the material parameters σ_f, τ_f, E_m and G_{II}.

7. ACKNOWLEDGEMENTS

REFERENCES

1. Takaku, A. and Arridge, R.G.C., "The Effect of Interfacial Radial and Shear Stress on Fibre Pull-out in Composite Materials", J. Phys. D: Appl. Phys. 6 (1973) 2038-2047.

2. Kaelble, D.H., "Theory and Analysis of Fracture Energy in Fiber Reinforced Composites", J. Adhesion 5 (1973) 245-264.

3. Greszczuk, L.B., "Theoretical Studies of the Mechanics of Fiber-Matrix Interface in Composites", Interfaces in Composites, ASTM STP 452, American Society for Testing and Materials, (1969), pp.42-58.

4. Lawrence, P., "Some Theoretical Considerations of Fibre Pull-out from an Elastic Matrix", J. Mater. Sci. 7 (1972) 1-6.

5. Outwater, J.O. and Murphy, M.C., "On the Fracture Energy of Uni-directional Laminates", 24th Annual Technical Conference, Reinforced Plastics/Composites Division. Paper 11c (Society of the Plastics Industry Inc. 1969).

6. Broutman, L.J., "Measurement of the Fiber-Polymer Matrix Interfacial Strength", Interfaces in Composites, ASTM STP 452, American Society for Testing and Materials, (1969), pp.27-41.

7. Harris, B., Beaumont, P.W.R. and Moncunill de Ferran, E., "Strength and Fracture Toughness of Carbon-Fibre Polyester Composites", J. Mater. Sci. 6 (1971) 238-251.

8. Marston, T.U., Atkins, A.G. and Felbeck, D.K., "Interfacial Fracture Energy and the Toughness of Composites", J. Mater. Sci. 9 (1974) 447-455.

9. Jayatilaka, A. De S. and Trustrum, K., "Statistical Approach to Brittle Fracture", J. Mater. Sci. 12 (1977) 1426-1430.

10. Kirk, J.N., Munro, M. and Beaumont, P.W.R., "The Fracture Energy of Hybrid Carbon and Glass-Fibre Composites", J. Mater. Sci. 13 (1978) 2197-2204.

11. Harris, B., Morley, J. and Phillips, D.C., "Fracture Mechanisms in Glass-Reinforced Plastics", J. Mater. Sci. 10 (1975) 2050-2061.

12. Kelly, A., "Interface Effects and the Work of Fracture of a Fibrous Composite", Proc. Roy. Soc. Lond. A. 319 (1970) 95-116.

13. Wagner, H.D., Tuler, F.R. and Marom, G., "Failure Analysis of Uni-directional Glass-reinforced Brittle Matrix Composites by the Fault Technique", J. Mater. Sci. 14 (1979), p.500-502 (Letters).

14. Beaumont, P.W.R. and Anstice, P.D., "A Failure Analysis of the Micromechanisms of Fracture of Carbon Fibre and Glass Fibre Composites in Monotonic Loading", J. Mater. Sci. 15 (1980) 2619-2635.

15. Anstice, P.D. and Beaumont, P.W.R., "Hygrothermal Effects on the Micromechanisms of Crack Extension in Glass-Fibre and Carbon-Fibre Composites", Proceedings of 5th International Congress on Fracture, Vol. I, p.473-483, Cannes, April 1981 (Pergamon Press).

TABLE 1 – The dependence of debonding stress on wire diameter

Diameter of wire/mm	0.79	0.23
Debonding Stress/GPa	0.68 (±0.06)	1.66 (±0.3)

TABLE 2 – Approximate expressions for the dependence of the average values of length distributions on the Weibull parameter, m

	APPROXIMATE EXPRESSION	RANGE OF VALID 'm'	TYPICAL 'm' VALUE (14)
PULL-OUT	$\overline{\ell^2} = \left\lvert 1.6\, m^{(-0.32)}\, \overline{\ell} \right\rvert^2$	$1.5 < m < 2$	1.9
DEBONDING	$\overline{\ell^2} = \left\lvert 1.2\, m^{(-0.11)}\, \overline{\ell} \right\rvert^2$ $\overline{\ell^3} = \left\lvert 1.4\, m^{(-0.18)}\, \overline{\ell} \right\rvert^3$	$2 < m < 5.5$	4.3

TABLE 3 – The default values of material constants

	Glass-Fibre	Carbon-Fibre
Diameter, $d/\mu m$	14	8
Strength, σ_f/GPa	1.65	3.12
Modulus, E_f/GPa	70	230
Interface parameter, G_2/Jm^{-2}	210	1950
Shear stress, τ_f/MPa	4	4
Volume fraction, V_f	0.5	0.5

Fig. 1   The debonded fibre. The linear build-up in stress with increasing x is given by equation 3.

Fig. 2   The relationship between the cumulative probability of failure of a fibre, P(σ), and the cumulative probability of fibre pull-out lengths.
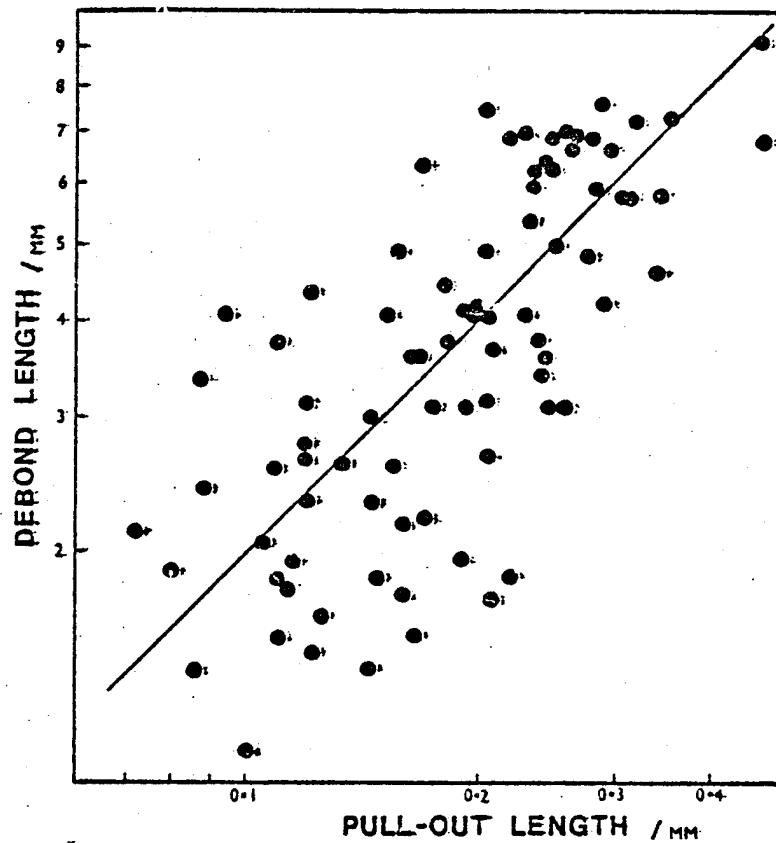
Fig. 3   Debond lengths versus average pull-out lengths, for glass-
         fibres in epoxy. The material was exposed to extremes of
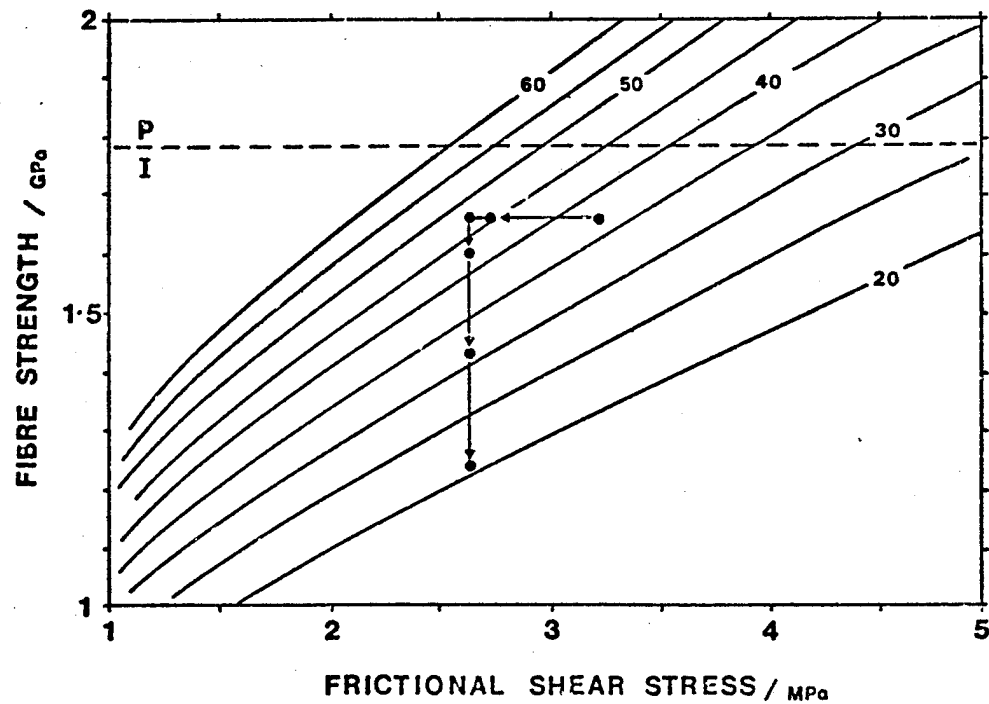   temperature and humidity, which is the cause of scatter.

Fig. 4   Contours of predicted toughness (units of KJ m^{-2}) for glass
         fibres in epoxy, as a function of fibre strength and frictional
         shear stress. The dashed line indicates a change in dominant
         toughening mechanism from Post debond friction (P), to Inter-
         facial energy (I). The changes of σ_f and τ_f for samples
         exposed to moisture are also shown.
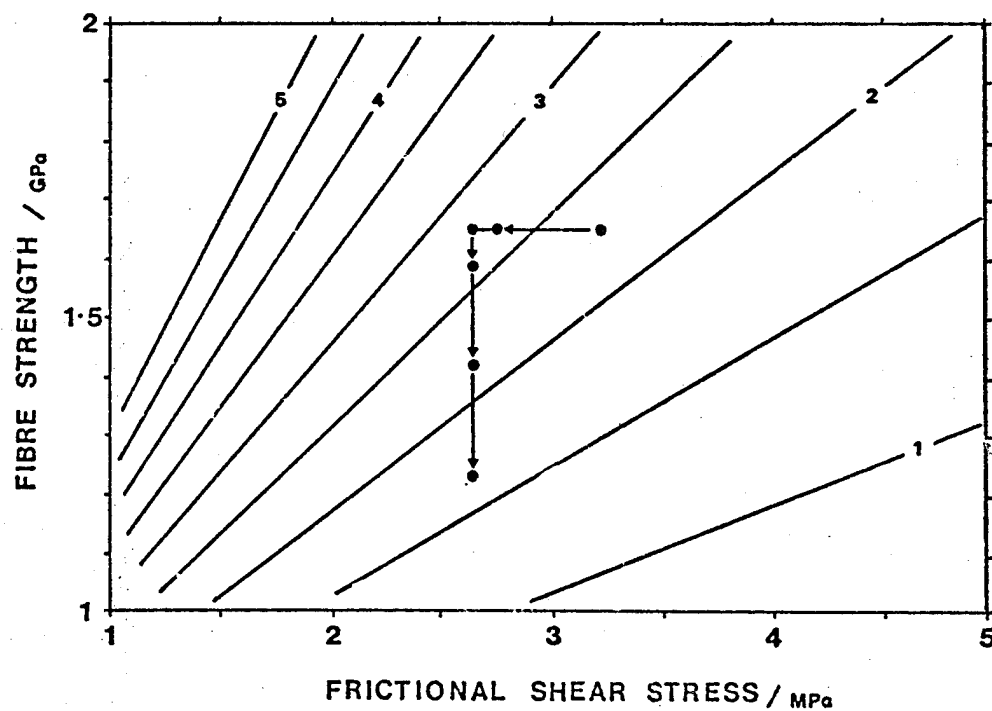
Fig. 5   Contours of predicted fibre debond length (units of millimetres)
         for glass-fibres in epoxy, as a function of fibre strength and
         frictional shear stress. The variation of σ_f and τ_f for
         samples exposed to moisture is also shown
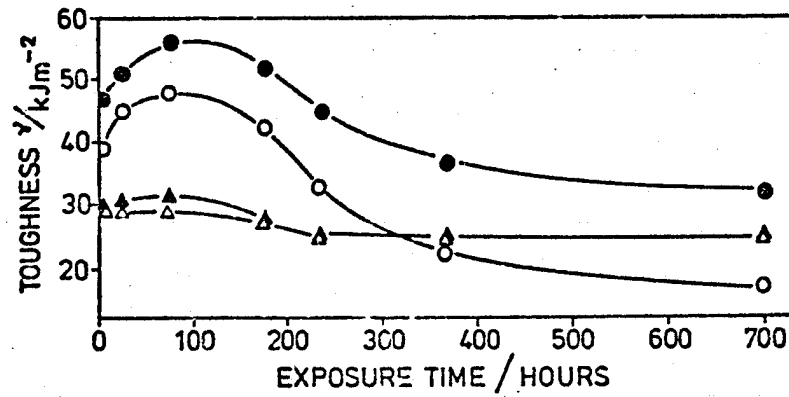
Fig. 6   The experimental (solid symbol) and theoretical (open symbol)
          toughness of glass-fibres (circles), and carbon-fibres
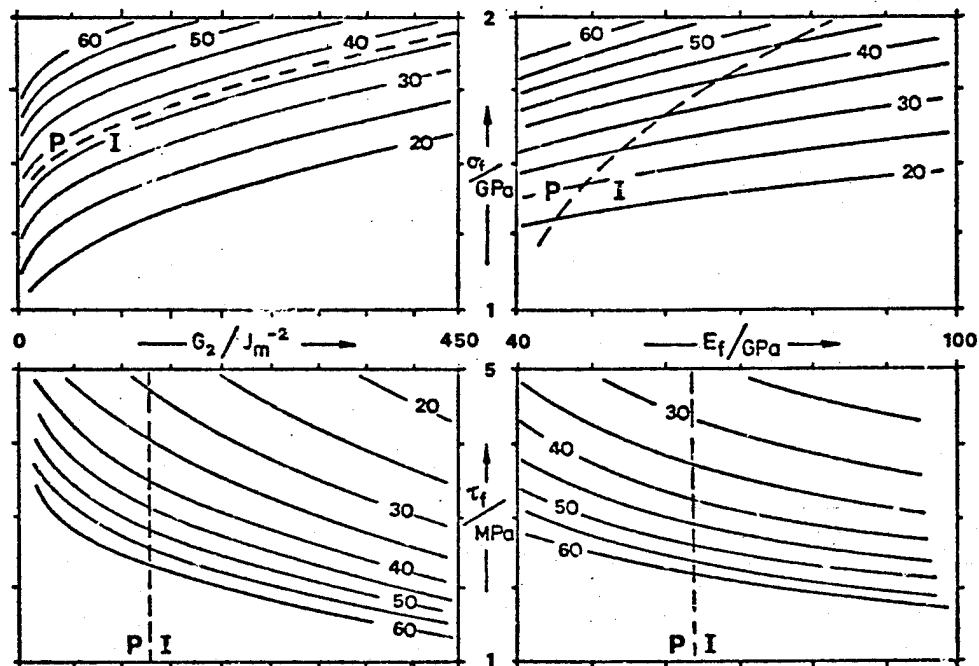   (triangles), in epoxy.

Fig. 7   Contours of toughness (units of KJ m^{-2}) for glass-fibres in
          epoxy as a function of fibre strength, fibre modulus, frictional
          shear stress and interface parameter. The dashed line indicates
          a change in the dominant toughening mechanism from Post debond
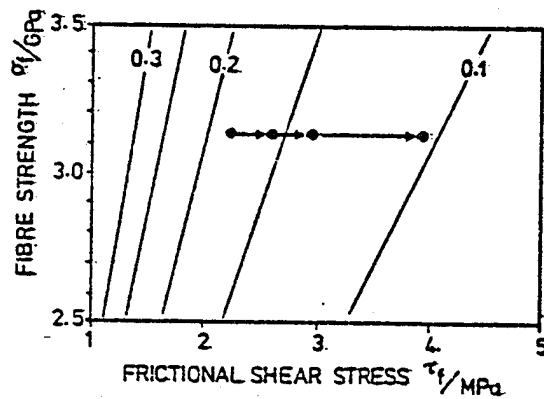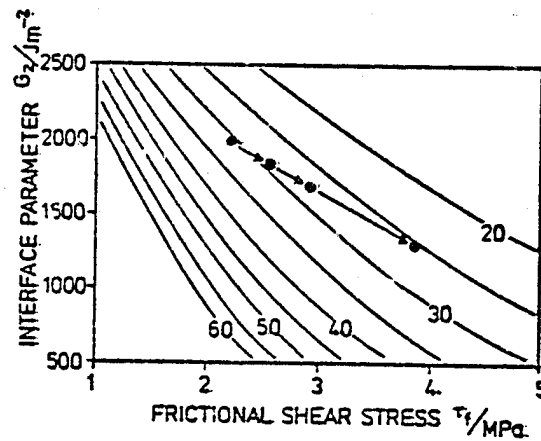   friction (P) to Interfacial energy (I).

Fig. 8   Contours of predicted toughness (units of KJm^{-2}) for carbon-fibres in epoxy. The variation of G_2 and τ_f for samples exposed to moisture is also shown. Interfacial energy is the dominant toughening mechanism.

Fig. 9   Contours of predicted fibre pull-out length (units of millimetres) for carbon-fibres in epoxy. The variation of G_2 and τ_f for samples exposed to moisture is also shown.